Appl. Phys. B (2014) 117:1065–1071
DOI 10.1007/s00340-014-5927-6

Applied Physics B
Lasers and Optics

Single-mode lasing from dye-doped holographic polymer-dispersed liquid crystal transmission gratings

Wenbin Huang · Quan Liu · Li Xuan · Linsen Chen

Received: 13 May 2014 / Accepted: 12 September 2014 / Published online: 7 October 2014

Abstract We demonstrate single-mode laser operation in dye-doped holographic polymer-dispersed liquid crystal (HPDLC) transmission gratings. The gratings are fabricated in cells made from specifically chosen glass substrates to decrease the refractive index difference between the waveguide core layer and cladding layer. The phase separation degree of liquid crystal after holographic recording is further optimized to confine only the lowest propagation mode in the device. The mode selection mechanism is explained under the framework of the waveguide distributed feedback (DFB) theory. The wavelength of single-mode lasing can be tuned between 620 and 660 nm by varying the grating period. Our results show the HPDLC technique could provide single-mode organic DFB lasers in a tunable, simple, and large-area manner.

W. Huang · L. Chen
College of Physics, Optoelectronics and Energy and Collaborative Innovation Center of Suzhou Nano Science and Technology, Soochow University, Suzhou 215006, China

W. Huang · L. Chen (✉)
Key Lab of Advanced Optical Manufacturing Technologies of Jiangsu Province and Key Lab of Modern Optical Technologies of Education Ministry of China, Soochow University, Suzhou 215006, China
e-mail: lschen@suda.edu.cn

Q. Liu · L. Xuan
State Key Laboratory of Applied Optics, Changchun Institute of Optics, Fine Mechanics and Physics, Chinese Academy of Sciences, Changchun 130033, China

Q. Liu
University of Chinese Academy of Sciences, Beijing 100039, China

1 Introduction

Over the last two decades, organic lasers have gained enormous research interest for their potential application in various fields including spectroscopy [1], chemical sensing [2], and data communication [3]. Motivation for these extensive studies on organic lasers was provided by many salient features of the organic gain medium [4], such as large stimulated emission cross sections, broad fluorescence spectra, low cost in terms of both processing techniques and materials, and easiness to tune the chemical structure for desired properties. Among the various resonator structures used in organic lasers, the distributed feedback (DFB) configuration, in which optical feedback is provided by the periodic, wavelength-scale microstructure, has proved particularly successful [5].

There is one type of DFB organic laser that has attracted special attention: the tunable DFB cavity based on liquid crystal (LC). LCs are molecules with large optical and dielectric anisotropies, which make them sensitive to various external stimuli. Thus, the orientational distribution of LC directors in these organic lasers could be easily altered, leading to lasing wavelength tuning within the emission spectrum of the gain medium. To date, there are several approaches to incorporate LCs into DFB cavities. Chiral LCs, in which LCs are self-organized to form a periodic structure, are a natural DFB resonator. Laser emission has been observed in dye-doped cholesteric LCs [6–8] or ferroelectric LCs [9], and broadband tunability can be conveniently achieved in these systems [10]. There are also demonstrations of tunable lasing in nano-imprinted structures infiltrated with nematic LC, in which LC may function as the waveguide core layer [11, 12] or the cladding layer [13]. Further, the dye-doped nematic LC layer could be directly pumped using holographic exposure apparatus

[14] or a shadow mask [15] and electrically tunable, single-mode DFB laser emission is possible.

Holographic polymer-dispersed liquid crystal (HPDLC) gratings, which are formed by photo-polymerization-induced phase separation of LC lamellas from the polymer matrix, are wavelength-scale, periodic structures with intrinsic embedded LCs [16]. Considering the simplicity and high throughput of HPDLC fabrication, these gratings have potential for realizing low-cost, tunable DFB laser sources [17]. Despite the intense studies into output properties, including switchability [18, 19] and tunability [20–23], lasing from dye-doped HPDLC gratings is usually multimode [20, 22, 24] as a result of weak mode selection capability. From the device application point of view, a single-mode HPDLC laser is more desirable. In this work, we demonstrate single-mode laser operation in a dye-doped HPDLC transmission grating. By decreasing the refractive index (RI) difference between the waveguide core layer and the cladding layer which is achieved by using suitable substrate glasses and optimizing the LC phase separation degree of the grating, it is able to confine only the lowest (zeroth) propagation mode in the device.

2 Experimental details

2.1 Materials and device structure

The homogeneous prepolymer syrup, which consisted of 28.5 wt% monomer dipentaerythritol hydroxyl pentaacrylate (DPHPA), 29 wt% monomer phthalic diglycol diacrylate (PDDA), 10 wt% cross-linking monomer *N*-vinylpyrrolidone (NVP), 0.5 wt% photoinitiator Rose Bengal (RB), 1.5 wt% coinitiator *N*-phenylglycine (NPG), 30 wt% nematic LC TEB30A (ordinary RI $n_o = 1.522$; extraordinary RI $n_e = 1.692$), and 0.5 wt% laser dye 4-dicyanomethylene-2-methyl-6-(p-dimethylaminostyryl)-4H-pyran (DCM), was introduced into empty cells by capillary suction in the dark. The samples were then exposed to the interference pattern created by two coherent laser beams (CW; $\lambda_w = 532$ nm). Recording beams were set to be S-polarized using half-wave plates to ensure high pattern contrast for efficient LC phase separation. The intersection angle θ between the two beams can be conveniently changed and precisely controlled within the error of 0.04°. The grating period can be calculated using $\Lambda = \lambda_w / 2\sin\left(\frac{\theta}{2}\right)$. The intensity for each beam was varied between 4 and 11 mW/cm^2, and the exposure time was around 3 min.

The device structure is schematically shown in Fig. 1. After the anisotropic photo-polymerization induced phase separation, the laser dye is naturally doped into the HPDLC

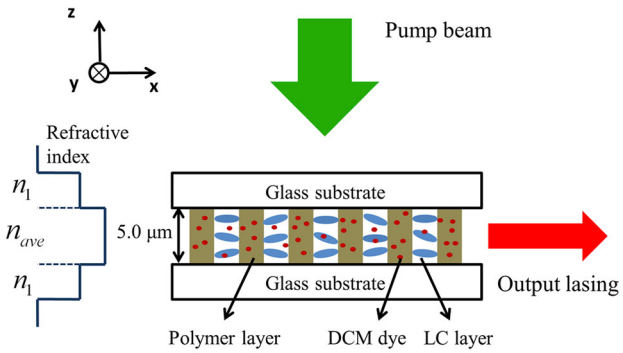

Fig. 1 Schematic illustration of the waveguide DFB structure

grating, and the grating layer serves not only as the feedback component but also as the gain medium. Since the RI of the HPDLC layer is higher than that of the glass substrate, DFB lasing modes can be bounded in this cavity and will not leak out through glass substrates. This working mechanism is referred to as the waveguide DFB scheme [5]. The number of lasing modes depends on the effective thickness of the core layer, and there are two possible approaches to achieve single-mode laser action [25]. One is by reducing the geometrical thickness of the core layer, which is the HPDLC grating in this case, and the other is by decreasing the RI difference between the cladding layer and the core layer. The first approach requires a thickness of the grating layer being <1 μm. Regardless of the difficulty in fabricating cells with such a small cell gap, the short absorption distance under transverse pumping cannot provide sufficient gain and thus would lead to a significant increase in the laser threshold. In this study, the second approach is employed, and two types of cells were made either by common K9 glasses (RI = 1.516) or by specifically chosen barite crown glasses BaK2 (RI = 1.53996). The RI of BaK2 glasses is very close to that of the HPDLC grating layer (around 1.541) [20], thereby minimizing the RI difference between the two layers. Ultrasonic washing in acetone and alcohol several times is used to clean these glass substrates. No further surface treatment is employed. The cell gap was controlled as 5 μm by Mylar spaces.

2.2 Optical characterizations

The devices were optically pumped using the linearly polarized output from a frequency-doubled Q-switched Nd:YAG laser (wavelength: 532 nm; pulse duration: 8 ns; and repetition rate: 1 Hz). The pump laser beam is 45° polarized with respect to the z-axis, and a set of calibrated neutral density filters was used to control incident pump energy. A spherical lens with a focal length of 20 mm was used to focus the pump beam into a roughly circular spot (1 mm diameter) to eliminate the adverse effect caused by cell gap inhomogeneity. Edge emission from the device

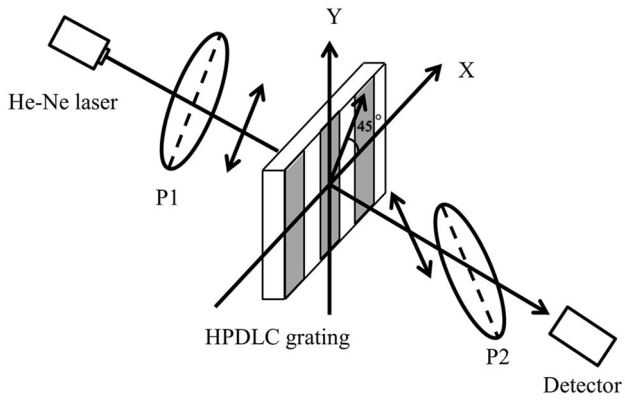

Fig. 2 Experimental setup for measuring the LC phase separation degree. P1 and P2 are two orthogonally aligned polarizers. The HPDLC grating is placed in a way that the angle between the grating vector and the transmission axis of either polarizer is 45°

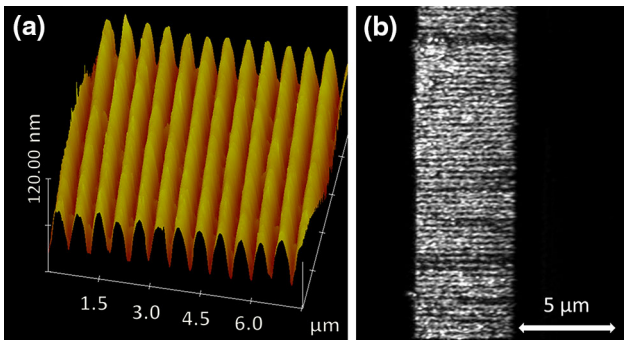

Fig. 3 Photographs of the scaffolding morphology HPDLC grating. **a** AFM image of the surface profile and **b** LSCM image of the grating cross section

was collected by a spherical lens and analyzed using a fiber-coupled spectrometer with a resolution of 0.2 nm, while lasing energy was measured using a Coherent J-10SI-HE energy meter.

According to previous studies on grating morphology [26, 27], the fabricated HPDLC grating under low curing intensity with acrylate monomers exhibits polymer scaffolding morphology. The phase-separated LCs are well aligned along the grating vector as shown in Fig. 1. The experimental setup for measuring the LC phase separation degree β (volume ratio of phase-separated LCs to total LCs) is shown in Fig. 2. The sample was situated between two orthogonally aligned polarizers, and a He–Ne laser at 633 nm was used as the incident beam. The angle between the grating vector and the transmission axis of either polarizer is 45°. The intensity of transmitted light depends sensitively on the phase retardation imposed by the well-aligned phase-separated LC molecules in the grating. We have [27]:

$$\beta = \frac{\lambda_{\mathrm{He-Ne}} \arcsin \sqrt{\frac{I_{\mathrm{T}}}{I_{\mathrm{OT}}}}}{\pi \varphi_{\mathrm{LC\_total}} \Delta n_{\mathrm{LC\_bulk}} L} \quad (1)$$

where $\lambda_{\mathrm{He-Ne}}$ is the output wavelength of the He–Ne laser, $\varphi_{\mathrm{LC\_total}}$ is the volume concentration of total LC in the prepolymer syrup, $\Delta n_{\mathrm{LC\_bulk}}$ is the birefringence of bulk nematic liquid crystal, L is the cell gap, I_{T} is the transmitted intensity through orthogonally aligned polarizers, and I_{OT} is the total intensity transmitted through the sample.

3 Results

3.1 HPDLC grating with low scattering loss

Figure 3 shows morphological images of the fabricated HPDLC grating where phase-separated LCs have been removed by ethanol. Figure 3a is an atomic force microscopy (AFM) photograph showing the surface profile of the grating. The surface appears to be rather smooth, without the presence of irregular bumps dwelled previously by LC domains. This non-droplet HPDLC morphology is termed as the polymer scaffolding morphology [26] in which there are numerous polymer filaments across the homogeneous LC layer. Thanks to the absence of LC droplet domains, the grating shows merely scattering loss (<5 %) and is quite suitable for use as a laser cavity. Figure 3b shows the cross section of the grating by using the laser scanning confocal microscopy (LSCM). The optical measurement could show the actual HPDLC grating morphology to a great degree, as the incident probing photons would not smear the organic grating which is often the case with high-energy electrons in scanning electron microscopy analysis. The grating depth is 5 μm, and it penetrates through the whole HPDLC film. Although the picture quality is limited by the spatial resolution of the LSCM (0.12 μm), we can find the LC layers are almost homogenous and contain merely spherical domains which is consistent with the smooth surface profile shown in Fig. 3a.

3.2 Single-mode lasing properties

When incident pump energy exceeds the laser threshold, the device emits lasing. Figure 4 shows the spectra of laser emission from both types of glass cells where the grating period is 602.4 nm. The samples were pumped at twice the corresponding threshold energy. Five lasing peaks which span from 612.2 to 620.6 nm can be found in the spectrum of the K9 glass cell. The wavelength separation between adjacent modes slightly decreases toward the long wavelength band. In distinct contrast, there is only one narrow lasing peak locating at 618.5 nm in the spectrum of the BaK2 glass cell, and thus, the spectral purity is much better in this case. We also show in Fig. 5 that single-mode laser

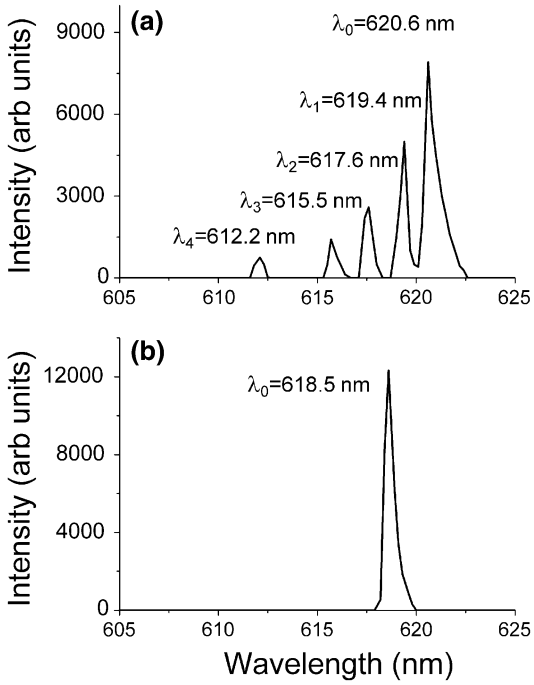

Fig. 4 Spectra of the lasing **a** from the common K9 glass cell; **b** from the Bak2 glass cell pumped at 2× corresponding threshold energy

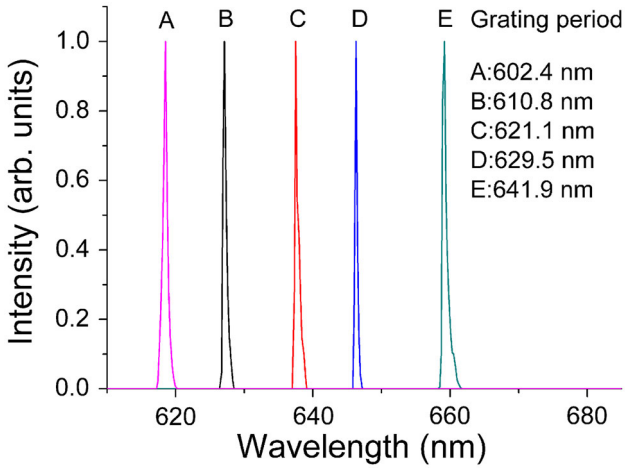

Fig. 5 Single-mode lasing from dye-doped transmission gratings with different grating periods

action can be obtained in the wavelength range between 620 and 660 nm by varying the grating period. Considering the lasing wavelength of each dye-doped HPDLC grating can be continuously tuned under applied electric field over a range of 10 nm [20], it is convenient to integrate several HPDLC gratings together to obtain single-mode lasing across the whole band range of the gain medium.

Figure 6 shows the dependence of output energy on input energy for the single-mode lasing. The laser threshold

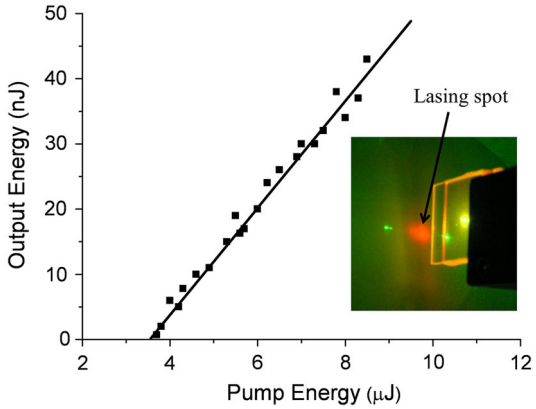

Fig. 6 Single-mode lasing energy as a function of pump energy. The *inset* shows the emission photograph of the single-mode lasing

is around 3.5 μJ/Pulse, which is a typical value in DFB lasers based on dye-doped HPDLC gratings [19, 28]. The working threshold in this paper merely changes as it mainly relies on the thickness and scattering loss of the grating film. The curve also shows the lasing slope efficiency is about 0.8 %. To date, there is only one report on the slope efficiency for the lasing from dye-doped HPDLCs, which is only around 0.1 % [18]. The lasing efficiency is much improved in our device as the HPDLC transmission grating we have employed shows merely scattering loss. The inset in Fig. 6 is an emission image of the device, in which a sharp lasing spot can be clearly seen. The divergence angles of the laser emission were estimated to be ∼0.16 and ∼0.20 rad in the directions parallel and perpendicular to the glass substrate, respectively.

4 Discussions

4.1 Effect of the LC phase separation degree

We found the high RI glass substrate alone cannot ensure single-mode laser action. Figure 7 shows the lasing spectra from dye-doped HPDLC gratings in BaK2 glass cells at various LC phase separation degrees pumped at a pump energy of 8 μJ/Pulse. Various lasing peaks with a line width of about 0.5 nm (close to the resolution of the used spectrometer) can be easily recognized. Output lasing becomes multimode when β is below 0.4. The spacing between adjacent modes is quite narrow (<1 nm), unlike the situation in Fig. 4a. Single-mode laser operation can be observed in Fig. 7c where the LC phase separation is comparatively more complete.

To explain the above results, the effect of the LC phase separation degree on the RI of the HPDLC film has to be taken into consideration. As the phase separation process in these gratings is driven by photo-induced anisotropic

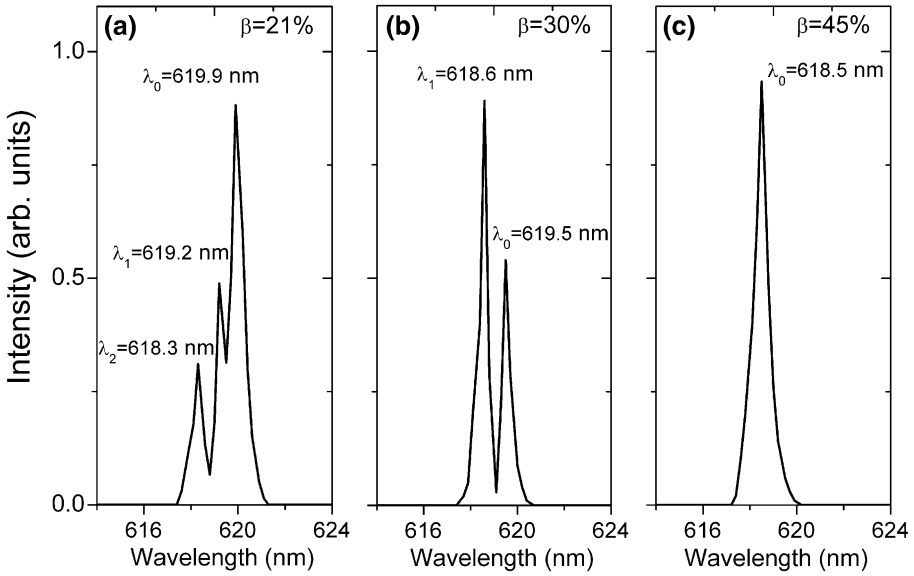

Fig. 7 Emission spectra of dye-doped HPDLC transmission gratings in BaK2 glass cells at various LC phase separation degrees pumped at 8 μJ/Pulse. The grating period is 602.4 nm

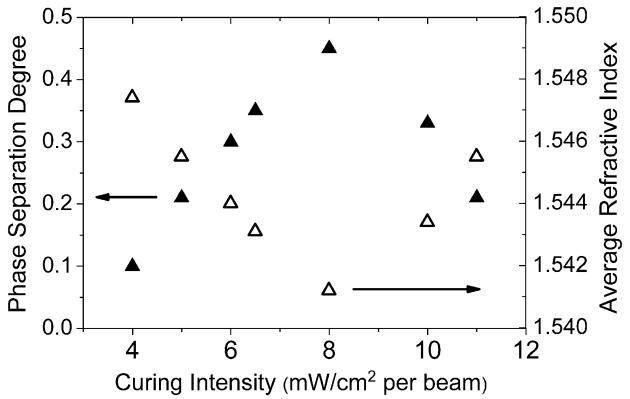

Fig. 8 Performance of the HPDLC grating as a function of curing intensity: *Solid triangles* represent the phase separation degree; *hollow triangles* represent the calculated grating refractive index

polymerization, β is very sensitive to exposure conditions. The measured phase separation degree β as a function of curing intensity is shown in Fig. 8, and it reaches a peak at a curing intensity of 8 mW/cm^2 per beam. For feedback light with a TE/TM polarization propagating along the grating vector, the average grating RI n_{ave} can be calculated using

$$n_{ave} = \left[n_p^2 \times \varphi_p + n_o^2 \times \beta \times (1-\varphi_p) + n_{iso}^2 \times (1-\beta) \times (1-\varphi_p)\right]^{1/2} \quad (2)$$

where φ_p is the volume proportion of pure polymer in the grating and can be determined from the initial prepolymer syrup composition; $n_{iso} = (2/3n_o^2 + 1/3n_e^2)^{1/2}$, which is the space-averaged RI of nematic LC. The first term in the latter part of Eq. (2) represents the contribution of pure polymer to the HPDLC film RI. The second term represents the well-aligned phase-separated LCs, while the third term indicates the contribution of dissolved LCs in the polymer matrix. The calculated n_{ave} as a function of curing intensity is also shown in Fig. 8. Thus, by controlling the LC phase separation degree through curing intensity, the average grating RI could be fine-tuned within 0.01.

4.2 Laser modes modeling in the waveguide DFB structure

We then modeled the allowed laser modes using the waveguide DFB theory. The essential physical conception behind this theory is that the lasing wavelength not only has to be the allowed guiding mode in this symmetric waveguide, but also it should fulfill the Bragg condition to be scattered backward by the periodic structure. From the investigation in Fig. 8, the average RI of the HPDLC grating is always higher than that of the BaK2 substrate, even at the phase separation degree peak. Thus, a total internal reflection condition can be always fulfilled within the symmetric waveguide structure, in which the grating serves as the core layer and the substrate serves as the cladding layer. Waveguiding modes could then be effectively confined in the dye-doped HPDLC grating without the loss through top and bottom substrates. Accordingly, the wavelength λ of possible lasing modes should first satisfy the waveguiding equation [29] (for TE modes):

$$\frac{\pi L}{\lambda}\sqrt{n_{ave}^2 - n_{eff\_mode}^2} = \frac{m_{mode}\pi}{2} + \arctan\sqrt{\frac{n_{eff\_mode}^2 - n_{glass\_substrate}^2}{n_{ave}^2 - n_{eff\_mode}^2}} \quad (3)$$

where L is the grating thickness, n_{ave} is the average refractive index of the HPDLC film, n_{eff_mode} is the

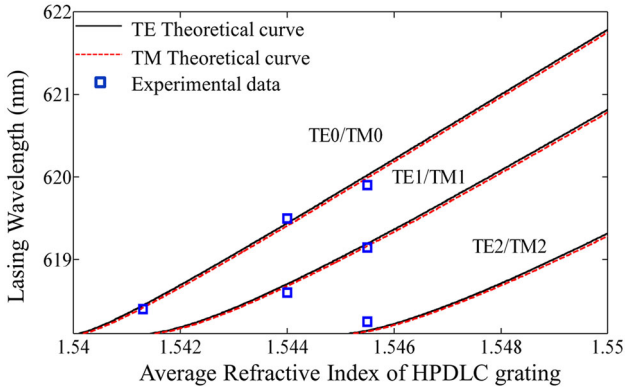

Fig. 9 Allowed DFB lasing wavelengths in the waveguide as a function of the average refractive index of the HPDLC grating: The continuum curve (*dashed curve*) is for TE (TM) lasing; *open squares* are experimental data

effective RI of the light mode in the waveguide, $n_{\text{glass\_substrate}}$ is the RI of the glass substrate, and m_{mode} (0, 1, 2 …) is the order of the waveguide mode. Apart from this equation, the lasing wavelength λ should obey the Bragg equation of this periodic structure, so that the backward-scattered light at each corrugation could combine together coherently and provides efficient feedback. In this way, a substantial optical gain through stimulated emission can be anticipated, which leads to the occurrence of laser action. We have [30]:

$$m\lambda = 2n_{\text{neff\_mode}}\Lambda \tag{4}$$

where m is the Bragg order (=3 in this work) and Λ is the grating period. By combing Eqs. (3, 4) together, the dependence of allowed lasing wavelength λ on the average RI of the HPDLC film n_{ave} can be numerically solved and is shown in Fig. 9. Recently, we have shown that better agreement with experiments can be obtained using the anisotropic DFB waveguide theory [31]. The isotropic one is sufficient for use here, as we concern no rotation of LC molecules and the traveling angle displacement between different modes is small (<3°). Experimental data in Fig. 7 are given as hollow squares in Fig. 9, and good agreement with the theoretical curves is obtained. For a more complete understanding of the spectral properties, the theoretical curve for TM lasing peaks is also shown in dotted line. It can be seen that TE and TM lasing belonging to the same propagating mode lie almost at the same wavelength location and they appear as one lasing peak in the output spectrum shown in Fig. 7. The modeling further confirms that a high LC phase separation degree is required to ensure single-mode laser operation, because lasing could become multimode with a RI difference of 0.002 between the HPDLC film and the glass substrate. From the perspective of a good DFB laser, the high phase separation degree is also demanding, as a high grating RI contrast would increase the coupling coefficient of feedback light. Thus, this method can provide single-mode laser devices with good working characteristics.

5 Conclusions

In conclusion, single-mode laser operation has been demonstrated in dye-doped HPDLC transmission gratings. The RI difference between the HPDLC film and the glass substrate is fine-tuned to allow only the lowest guided mode to be confined. The lasing mode selection mechanism is explained on the basis of waveguide DFB theory. The low-loss polymer scaffolding morphology grating is quite suitable for use as a laser cavity: The single-mode lasing threshold is 3.5 μJ/Pulse, and the slope efficiency is 0.8 %.

Acknowledgments The authors are grateful for financial support from the Priority Academic Program Development of Jiangsu Higher Education Institutions (PAPD).

References

1. Y. Oki, S. Miyamoto, M. Maeda, N.J. Vasa, Opt. Lett. **27**, 1220 (2002)
2. Y. Yang, G.A. Turnbull, I.D.W. Samuel, Adv. Funct. Mater. **20**, 2093 (2010)
3. J. Clark, G. Lanzani, Nat. Photon. **4**, 438 (2010)
4. S. Chénais, S. Forget, Polym. Int. **61**, 390 (2012)
5. I.D.W. Samuel, G.A. Turnbull, Chem. Rev. **107**, 1272 (2007)
6. A.Y.-G. Fuh, T.-H. Lin, J.-H. Liu, F.-C. Wu, Opt. Express **12**, 1857 (2004)
7. B. Liu, Z. Zheng, X. Chen, D. Shen, Opt. Mater. Express **3**, 519 (2013)
8. M.I. Barnik, L.M. Blinov, V.V. Lazarev, S.P. Palto, B.A. Umanskii, N.M. Shtykov, J. Appl. Phys. **103**, 123113 (2008)
9. M. Ozaki, M. Kasano, D. Ganzke, W. Haase, K. Yoshino, Adv. Mater. **14**, 306 (2002)
10. T.-H. Lin, Y.-J. Chen, C.-H. Wu, A.Y.-G. Fuh, J.-H. Liu, P.-C. Yang, Appl. Phys. Lett. **86**, 161120 (2005)
11. R. Ozaki, T. Shinpo, K. Yoshino, M. Ozaki, H. Moritake, Appl. Phys. Express **1**, 012003 (2008)
12. L. Chen, Z. Liu, K. Che, Y. Bu, S. Li, Q. Zhou, H. Xu, Z. Cai, Thin Solid Films **520**, 2971 (2012)
13. S. Klinkhammer, N. Heussner, K. Huska, T. Bocksrocker, F. Geislhöringer, C. Vannahme, T. Mappes, U. Lemmer, Appl. Phys. Lett. **99**, 023307 (2011)
14. T. Matsui, M. Ozaki, K. Yoshino, Jpn. J. Appl. Phys. **42**, L1462 (2003)
15. L.M. Blinov, G. Cipparrone, A. Mazzulla, P. Pagliusi, V.V. Lazarev, S.P. Palto, Appl. Phys. Lett. **90**, 131103 (2007)
16. R.L. Sutherland, L.V. Natarajan, V.P. Tondiglia, Chem. Mater. **5**, 1533 (1993)
17. R. Jakubiak, T.J. Bunning, R.A. Vaia, L.V. Natarajan, V.P. Tondiglia, Adv. Mater. **15**, 241 (2003)
18. V.K.S. Hsiao, C. Lu, G.S. He, M. Pan, A.N. Cartwright, P.N. Prasad, R. Jakubiak, R.A. Vaia, T.J. Bunning, Opt. Express **13**, 3787 (2005)

19. Y.J. Liu, X.W. Sun, H.I. Elim, W. Ji, Appl. Phys. Lett. **90**, 011109 (2007)
20. W. Huang, Z. Diao, L. Yao, Z. Cao, Y. Liu, J. Ma, L. Xuan, Appl. Phys. Express **6**, 022702 (2013)
21. D.E. Lucchetta, L. Criante, O. Francescangeli, F. Simoni, Appl. Phys. Lett. **84**, 837 (2004)
22. D. Luo, X.W. Sun, H.T. Dai, H.V. Demir, H.Z. Yang, W. Ji, J. Appl. Phys. **108**, 013106 (2010)
23. R. Jakubiak, V.P. Tondiglia, L.V. Natarajan, R.L. Sutherland, P. Lloyd, T.J. Bunning, R.A. Vaia, Adv. Mater. **17**, 2807 (2005)
24. M.S. Li, A.Y.-G. Fuh, S.-T. Wu, Opt. Lett. **37**, 3249 (2012)
25. T. Matsui, M. Ozaki, K. Yoshino, J. Opt. Soc. Am. B **21**, 1651 (2004)
26. K.K. Vardanyan, J. Qi, J.N. Eakin, M.D. Sarkar, G.P. Crawford, Appl. Phys. Lett. **81**, 4736 (2002)
27. W. Huang, Y. Liu, Z. Diao, C. Yang, L. Yao, J. Ma, L. Xuan, Appl. Opt. **51**, 4013 (2012)
28. D.E. Lucchetta, F. Vita, R. Castagna, O. Francescangeli, F. Simoni, Photon. Nanostruct. Fundam. Appl. **10**, 140 (2012)
29. K. Okamoto, *Fundamentals of Optical Waveguides* (Academic press, Burlington, 2006)
30. H. Kogelnik, C.V. Shank, Appl. Phys. Lett. **18**, 152 (1971)
31. Z. Diao, W. Huang, Z. Peng, Q. Mu, Y. Liu, J. Ma, L. Xuan, Liq. Cryst. **41**, 239 (2014)